



## Soil hydrological properties regulate grassland ecosystem responses to multifactor global change: A modeling analysis

Ensheng Weng<sup>1,2</sup> and Yiqi Luo<sup>1</sup>

Received 29 June 2007; revised 24 February 2008; accepted 14 March 2008; published 11 July 2008.

[1] We conducted a modeling study to evaluate how soil hydrological properties regulate water and carbon dynamics of grassland ecosystems in response to multifactor global change. We first calibrated a process-based terrestrial ecosystem (TECO) model against data from two experiments with warming and clipping or doubled precipitation in Great Plains. The calibrated model was used to simulate responses of soil moisture, evaporation, transpiration, runoff, net primary production (NPP), ecosystem respiration ( $R_h$ ), and net ecosystem production (NEP) to changes in precipitation amounts and intensity, increased temperature, and elevated atmospheric  $[CO_2]$  along a soil texture gradient (sand, sandy loam, loam, silt loam, and clay loam). Soil available water capacity (AWC), which is the difference between field capacity and wilting point, was used as the index to represent soil hydrological properties of the five soil texture types. Simulation results showed that soil AWC altered partitioning of precipitation among runoff, evaporation, and transpiration, and consequently regulated ecosystem responses to global environmental changes. The fractions of precipitation that were used for evaporation and transpiration increased with soil AWC but decreased for runoff. High AWC could greatly buffer water stress during long drought periods, particularly after a large rainfall event. NPP,  $R_h$ , and NEP usually increased with AWC under ambient and 50% increased precipitation scenarios. With the halved precipitation amount, NPP,  $R_h$ , and NEP only increased from 7% to 7.5% of AWC followed by declines. Warming and  $CO_2$  effects on soil moisture, evapotranspiration, and runoff were magnified by soil AWC. Regulatory patterns of AWC on responses of NPP,  $R_h$ , and NEP to warming were complex. In general,  $CO_2$  effects on NPP,  $R_h$ , and NEP increased with soil AWC. Our results indicate that variations in soil texture may be one of the major causes underlying variable responses of ecosystems to global changes observed from different experiments.

**Citation:** Weng, E., and Y. Luo (2008), Soil hydrological properties regulate grassland ecosystem responses to multifactor global change: A modeling analysis, *J. Geophys. Res.*, 113, G03003, doi:10.1029/2007JG000539.

### 1. Introduction

[2] Increased concentration of carbon dioxide ( $[CO_2]$ ) in the atmosphere has resulted in increases in global surface temperature and altered precipitation patterns [IPCC, 2001]. Experimental and modeling studies have shown that terrestrial ecosystems have diverse responses to climate change. Experimental warming in a range of 0.3~6.0°C, for example, significantly increased soil respiration rates by 20% and plant productivity by 19% with considerable variation among individual sites [Rustad *et al.*, 2001]. Meta-analyses of data published in the literature about ecosystems responses to elevated  $[CO_2]$  revealed a wide range of

responses to increases in atmospheric  $[CO_2]$  [Jastrow *et al.*, 2005; Luo *et al.*, 2006], from no biomass responses in alpine grasslands [Körner *et al.*, 1997] and in the subhumid tall grass prairie for wet years [Owensby *et al.*, 1999], to consistent and substantial production responses in semiarid shortgrass steppe [Morgan *et al.*, 2004]. How to explain the variations in observed terrestrial ecosystem responses to climate change has been a great challenge in the research community.

[3] Various ecosystem responses to global change may be partially caused by soil hydrological properties at least for two reasons. First, soil water strongly regulates plant growth and primary productivity for most terrestrial ecosystems, particularly in arid and semiarid regions [Schulze *et al.*, 1987]. Second, all global change factors, such as climate warming, rising atmospheric  $CO_2$  concentration, and altered precipitation intensity and frequency, induce changes in soil water availability [Niklaus *et al.*, 1998; Wan *et al.*, 2002] and, therefore, indirectly affect plant and ecosystem processes [Saleska *et al.*, 1999; Shaver *et al.*, 2000; Morgan *et al.*

<sup>1</sup>Department of Botany and Microbiology, University of Oklahoma, Norman, Oklahoma, USA.

<sup>2</sup>Ministry of Education Key Laboratory for Biodiversity Science and Ecological Engineering, Fudan University, Shanghai, China.

*al.*, 2004; *Luo*, 2007]. However, how soil hydrological properties regulate ecosystem responses to global change factors, to the best of our knowledge, has not been well examined.

[4] Soil stores precipitation water for plant use over time and thus regulates partitioning of precipitation among alternative outflows such as runoff, evaporation, and transpiration [*Rodriguez-Iturbe and Porporato*, 2004]. The capability of soil to store water is mainly determined by soil texture and quantified by soil moisture release curves. Two points on soil moisture release curve are particularly important: field capacity and permanent wilting point. The difference between field capacity and wilting point defines available water capacity (AWC), the maximal amount of water that is available for plants. Soil texture varies greatly over spatial scales [*Miller and White*, 1998]. In the Northern Territory, Australia, for example, along the precipitation gradient from north to south, predominant soils in the wetter end of a precipitation gradient are loams and sands, and clay soils are more extensive in the drier sectors of the gradient [*Williams et al.*, 1996]. At a local scale, soil texture varies dramatically with landform [*Rosenbloom et al.*, 2001]. Variation in soil texture creates diverse soil moisture environments in an area even with the same amount of precipitation. In dry regions, for example, soil evaporation is lower in sandy soils than that in loamy soils [*Buckman and Brady*, 1960].

[5] Diverse soil hydrologic properties and water environments result in considerable variations in plant production and ecosystem function [*McAuliffe*, 2003]. Among the most noticeable hypotheses is the inverse-texture hypothesis (ITH) [*Noy-Meir*, 1973], which states that production is higher on coarse-textured soils than that on fine-textured soils in dry regions because the water availability will be high in coarse soil in dry regions. The hypothesis has been supported by many studies [e.g., *Sala et al.*, 1988; *Lane et al.*, 1998; *Epstein et al.*, 1997]. According to observations from central grassland regions in the United States, sandy soils are more productive than loamy soils when annual precipitation is less than 370 mm [*Sala et al.*, 1988]. However, when precipitation is more than 370 mm, sandy soils are less productive than loamy soils.

[6] In addition, soil hydrological properties likely regulate ecosystem responses to changes in precipitation patterns, temperature, and atmospheric [CO<sub>2</sub>]. General circulation models forecast a higher frequency of extreme rainfall events, a lower frequency of rainfall days, and longer intervals of dry periods [*Easterling et al.*, 2000]. It is well known that changes in precipitation directly alter soil water content and dynamics. An experimental study has demonstrated that increased temporal variability in precipitation and soil moisture increased plant water stress and reduced plant productivity [*Knapp et al.*, 2002]. It is not clear whether these experimental conclusions from the Konza prairie reserve can be generalized to other regions with different soil hydrological properties and climate regimes. Global warming and elevated atmospheric [CO<sub>2</sub>] also alter ecosystem water availability. Warming usually induces drought by increasing evapotranspiration [*Wan et al.*, 2002], leading to higher possibility of drought stress to terrestrial ecosystems [*Harte et al.*, 1995]. Elevated CO<sub>2</sub> usually results in increases in soil moisture by reducing leaf

stomatal conductance and mitigates plant water stress [*Knapp et al.*, 1993; *Owensby et al.*, 1999; *Morgan et al.*, 2004; *Moore and Field*, 2006]. It is not clear, however, how ecosystem responses to climate warming and elevated [CO<sub>2</sub>] vary with soil textures with distinct soil hydrological properties.

[7] In this paper, we conducted a modeling study to evaluate how soil textures with distinct hydrological properties regulate ecosystem water and carbon dynamics in response to altered precipitation amounts and frequencies, climate warming, and elevated atmospheric [CO<sub>2</sub>]. A process-based ecosystem model was first calibrated against data from two global change experiments in the Southern Great Plains, USA, before used to explore soil water dynamics and carbon processes in five soil types of grasslands. We chose grasslands for this study also partly because they are one of the most widespread ecosystems types worldwide, covering nearly 1/5 of the world's land surface where soil and climatic conditions are diverse [*Parton et al.*, 1995]. Many experiments have shown rapid and diverse responses of grasslands to changes in temperature, water, and atmospheric [CO<sub>2</sub>] [*Zavaleta et al.*, 2003; *Luo*, 2007]. This modeling study mainly addressed the following two questions. How did soil texture regulate partitioning of precipitation among runoff, evaporation, and transpiration? How did the changes in water partitioning affect ecosystem responses to changes in precipitation frequency and amount, warming, and elevated atmospheric [CO<sub>2</sub>]?

## 2. Material and Method

### 2.1. Terrestrial ECOSystem (TECO) Model

[8] The TECO model evolves from its precursor model TCS [*Luo and Reynolds*, 1999]. It is a process-based ecosystem model and designed to examine critical processes in regulating interactive responses of plants and ecosystems to elevated CO<sub>2</sub>, warming, altered precipitation. TECO has four major components: canopy photosynthesis, soil water dynamic, plant growth (allocation and phenology), and soil carbon transfers (Figure 1). The canopy photosynthesis and soil water dynamic submodels run at the hourly time step. The plant growth and soil carbon submodels run at the daily time step. The detailed description of the TECO model is in the appendix. Here is a brief description.

[9] The canopy photosynthesis was simulated by a multilayer process-based model, which mainly evolves from the model developed by *Wang and Leuning* [1998]. It simulates radiation transmission in the canopy based on Beer's law. Foliage is divided into sunlit and shaded leaves. Leaf photosynthesis is estimated based on the Farquhar photosynthesis model [*Farquhar et al.*, 1980] and a stomatal conductance model proposed by *Ball et al.* [1987]. The soil water dynamic submodel stratifies soil into ten layers. The thickness of the first layer is 10 cm and 20 cm for the other 9 layers. Soil water content of these layers is determined by mass balance between water influx and efflux. The water influx is precipitation for the surface layer and percolation for deeper layers. The water efflux includes evaporation, transpiration, and runoff. Evaporation is mainly controlled by the moisture of the first soil layer and evaporative demand of atmosphere. Transpiration is regulated by sto-

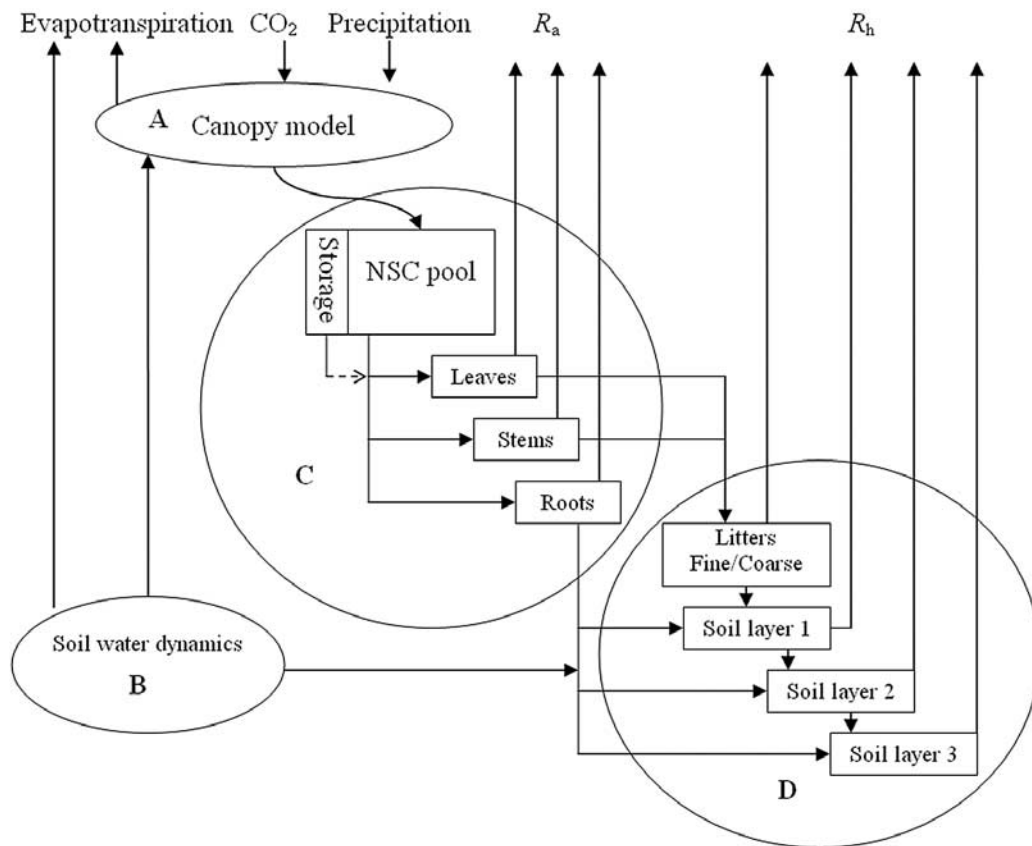


**Figure 1.** Schematic presentation of TECO model. (A) Canopy model, (B) Soil water dynamics model, (C) Plant growth model, and (D) Carbon transfer model. Rectangles represent the carbon pools. Soil is stratified into three layers.  $R_a$ : autotrophic respiration.  $R_h$ : heterotrophic respiration, NSC: nonstructure carbohydrate.

metal conductance, soil moisture, and root distribution. The plant growth submodel simulates carbon allocation and phenology following ALPHAPHA model [Luo *et al.*, 1995; Denison and Loomis, 1989] and CTEM [Arora and Boer, 2005], respectively. Allocation of assimilated carbon among the leaves, stems, and roots depends on their growth rates, and varies with phenology. Phenology is represented by annual variation of leaf area index (LAI). Leaf onset, the start of a growing season, is determined by growing degree days (GDD). Leaf senescence is induced by low temperature and low soil moisture. When LAI is below a certain level ( $LAI < 0.1$ ), the end of growing season comes. The carbon transfer submodel considers the movement of carbon from plant to soil through litterfall and the decomposition of litter and soil organic carbon [Luo and Reynolds, 1999; Barrett, 2002]. In this submodel, a soil profile is divided into three layers with carbon movement from upper to lower layers. Carbon inputs to the soil from root growth and dead root residues are partitioned into these three layers.

[10] Rooting depth and root vertical distribution define the soil volume from which plants potentially extract water. Most of the grass roots distribute in the soil layers less than 70 cm and the distribution of roots vary little with soil texture and soil moisture profiles [Jackson *et al.*, 1996; Nippert and Knapp, 2007; Singh *et al.*, 1998]. On the basis of patterns illustrated by the experimental data, maximum

rooting depth was assumed to be 70 cm, reaching to the fourth soil layer (50~70 cm) in our model. Root vertical distribution was dynamical, which varied with root growth and death in every soil layer. The initial ratios of roots in the four soil layers were set as 40% (0~10 cm), 40% (10~30 cm), 15% (30~50 cm), and 5% (50~70 cm). Variations in root biomass during simulations were limited within 20% of the initial ratios.

## 2.2. Model Calibration

[11] The TECO model was calibrated against observations from two global change experiments conducted in the Kessler Farm Field Laboratory (KFFL), University of Oklahoma. KFFL is located at the Great Plains Apiaries in McClain County, Oklahoma (34°59' N, 97°31' W), approximately 40 km southwest of the Norman campus of the University of Oklahoma, USA. It is an upland tallgrass prairie dominated mainly by  $C_4$  grasses. A silt loam soil in the grassland includes 35.3% sand, 55.0% silt, and 9.7% clay. The soil belongs to part of the Nash-Lucien complex with high water holding capacity (around 37%) and a deep, moderately penetrable root zone [Zhou *et al.*, 2007].

[12] The model was driven by the meteorological data from the nearest meteorological station, a MESONET station near Washington, Oklahoma, which includes records of temperature, precipitation, solar radiation, soil tempera-

**Table 1.** Treatment Levels of Five Variables Examined in This Study<sup>a</sup>

Variable	Treatment Level
Precipitation amount	ambient (1.0 P), halved (0.5 P), one and one half(1.5 P),
Precipitation intensity	ambient intensity, high intensity
Temperature	ambient, +2°C increased
CO <sub>2</sub> concentration	ambient concentration (360 ppm), doubled concentration (720 ppm)
Available water capacity	5%, 7.5%, 15%, 23%, 30%

<sup>a</sup>We used full factorial combinations of three variables (i.e., precipitation amount, precipitation intensity, and soil texture type) at ambient temperature and [CO<sub>2</sub>], warming, and elevated [CO<sub>2</sub>] to define 90 scenarios for this simulation study.

ture, and relative humidity. The data used to calibrate the model were measured soil respiration, soil moisture, above ground and below ground biomass during 2000~2005. Soil texture was assigned a field capacity of 37% and a wilting point of 10%. Thus the available water capacity was 27%. The model was run for 1200 years to reach an equilibrium state before used to simulate daily soil moisture, soil respiration, and aboveground biomass from 1/1/2000 to 12/31/2005 for calibration against the collected data.

[13] Comparison between model simulations and observations was evaluated by a number of statistical approaches

following *Hanson et al.* [2004]. Linear regression slopes, intercepts, and determinant coefficient ( $R^2$ ) were provided as an initial comparison between observations and predictions. Relative bias (RB) and mean absolute bias (ABS) were used to measure the magnitude of bias and the deviation from the observed values, respectively, which were calculated by the following equations.

$$RB = \frac{\sum(\hat{y}_i - y_i)}{\sum y_i} \times 100 \quad (1)$$

$$ABS = \frac{\sum|\hat{y}_i - y_i|}{n} \quad (2)$$

where  $\hat{y}_i$  represents simulated values and  $y_i$  measured values.

### 2.3. Scenarios

[14] This study examined five variables: precipitation amount, precipitation intensity, temperature, CO<sub>2</sub> concentration, and soil available capacity (AWC) (Table 1). We had three levels of precipitation amount (i.e., ambient, 0.5, and 1.5), two levels of precipitation intensity (i.e., ambient and high intensity), two levels of temperature (i.e., ambient and warming by 2°C), two levels of CO<sub>2</sub> concentration (360 and 720 ppm), and five levels of soil AWC (i.e., 5%,

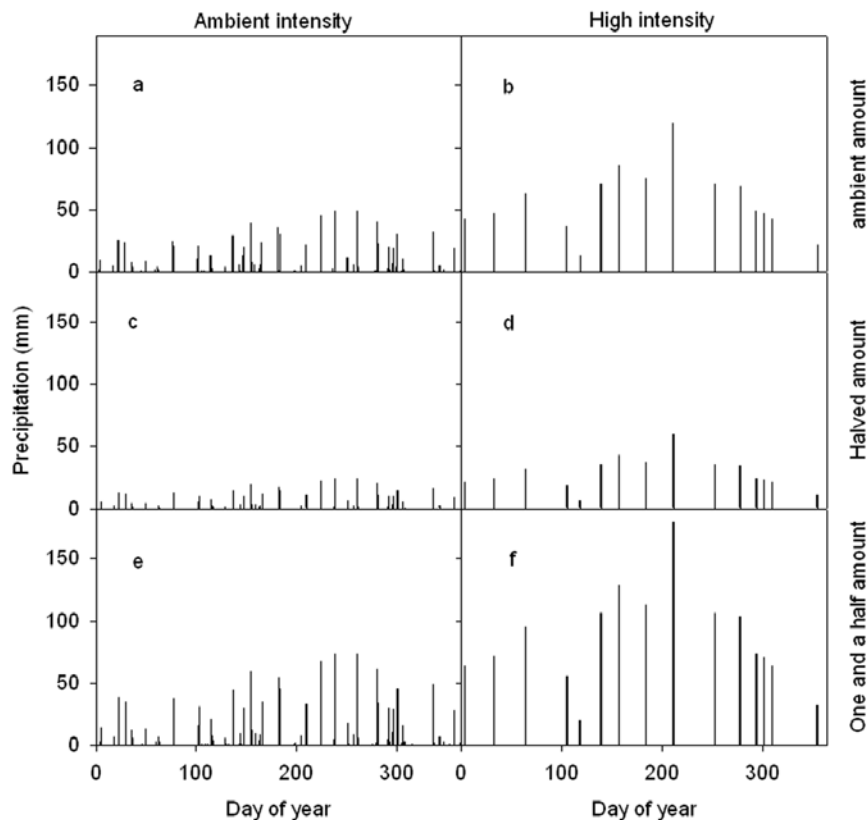


**Figure 2.** Scenarios of precipitation intensity and frequency. (a) Ambient precipitation (1.0 P), (b) precipitation with high intensity (the neighboring 6 times precipitation events were merged into one precipitation) (1.0 P), (c) halved precipitation with ambient frequency (0.5P), (d) halved precipitation with high intensity (0.5 P), (e) one-and-one-half precipitation with ambient intensity (1.5 P), (f) one-and-one-half precipitation with high intensity (1.5 P).

**Table 2.** Field Capacities, Wilting Points, and Available Water Capacities of Five Soil Texture Types<sup>a</sup>

Soil Texture	Sand	Sandy Loam	Loam	Silt Loam	Clay Loam
Field capacity, %	10.0	15.0	25.0	35.0	45.0
Wilting point, %	5.0	7.5	10.0	12.0	15.0
Available water capacity, %	5.0	7.5	15.0	23.0	30.0

<sup>a</sup>The available water capacities were used as five scenarios in this study.

7.5%, 15%, 23%, and 30%). A full factorial design of three variables (i.e., precipitation amount, precipitation intensity, and soil texture type) at ambient temperature and [CO<sub>2</sub>], warming, and elevated [CO<sub>2</sub>] defined 90 scenarios for this simulation study.

[15] We defined the ambient climatic scenario (i.e., ambient precipitation amount, ambient precipitation intensity, and ambient temperature) based on analysis of meteorological data recorded at Kessler Farm Field Laboratory during 2000–2005 while calibration data were available. During the period, the mean annual precipitation was 804 mm. The mean number of the days with precipitation in a year was 95. The precipitation during growing seasons from April to October was 582 mm, 72% of the annual

precipitation. The highest daily precipitation was 76.7 mm, which occurred on 30 August 2003. Most of the precipitation events had rainfall amounts below 10 mm (413 of 568 precipitation events in the 6 years). The daily precipitation with amounts above 50 mm occurred 8 times. The mean temperature was 16°C. The highest mean daily temperature was 32°C, and the lowest mean daily temperature was -9.9°C.

[16] In 2002, the precipitation was 854.5 mm and there were 89 rain days, both of which were the closest to the mean precipitation amount and the mean number of rain days during the 6 years. Thus the meteorological data in 2002 were used to define the ambient climatic scenario in this modeling study (Figure 2a). The 89 rain days were treated as 89 rainfall events. The mean precipitation per rainfall event of the ambient intensity was 9.6 mm and the mean length of intervals between rainfall events was 5 d.

[17] The high intensity level of precipitation was defined by merging the neighboring 6 rainfall events into one, reducing to 15 rainfall events (Figure 2b) from the 89 rainfall events in the ambient climate scenario. The mean precipitation intensity increased to 56.9 mm and mean length of intervals between precipitation events increased to 24 d in the high intensity level.

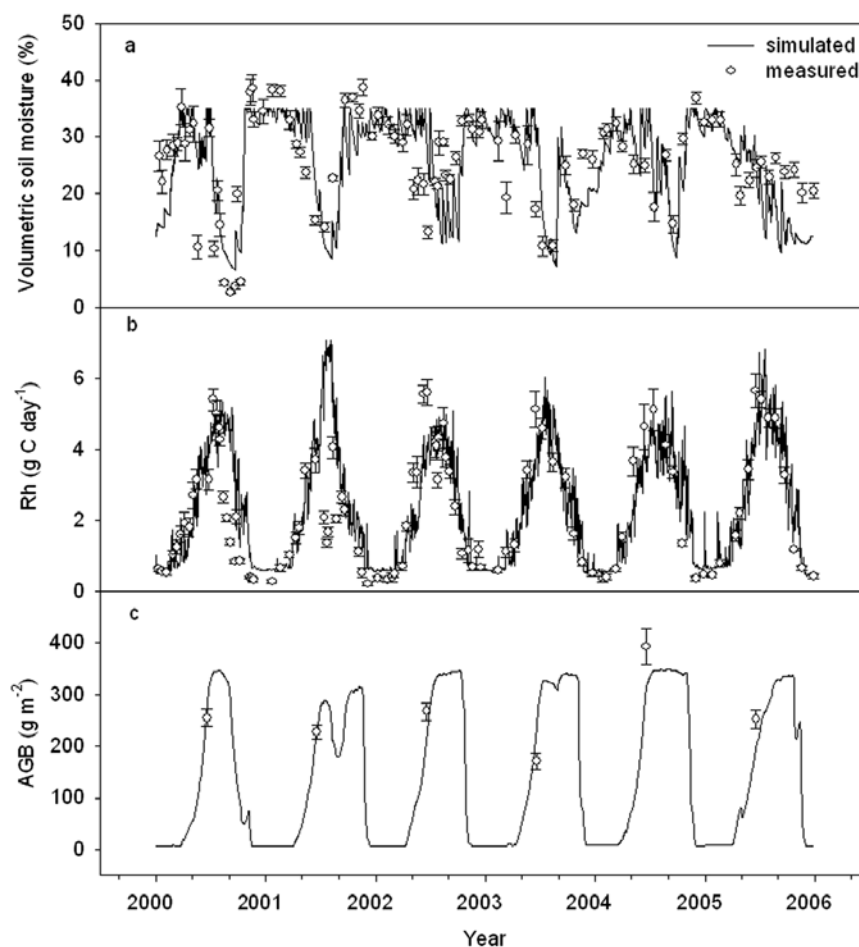


**Figure 3.** Model validations. (a) soil moisture, (b) soil respiration, and (c) aboveground biomass.  $R_h$  stands for heterotrophic respiration ( $\text{g C m}^{-2} \cdot \text{d}^{-1}$ ); AGB stands for above ground biomass ( $\text{g} \cdot \text{m}^{-2}$ ). The solid lines show simulated results. The open dots show the measured values.

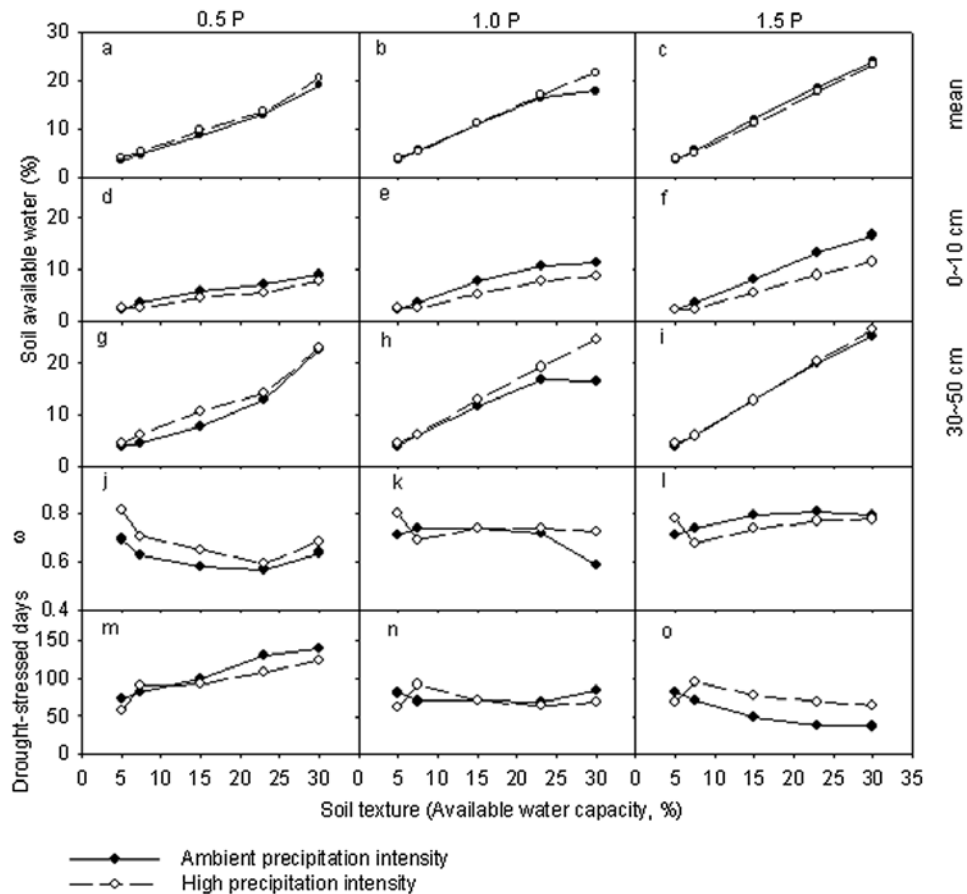


**Figure 4.** Soil available water, normalized soil moisture, and drought-stressed days with available water capacity at the three precipitation amount levels and two precipitation frequencies. Filled circles with solid lines represent ambient precipitation frequency. Open circles with dashed lines represent high precipitation intensity. Figures 4a, 4b, and 4c show mean soil available water in root zone (1~4 soil layers). Figures 4d, 4e, and 4f show soil available water of the surface layer (0~10 cm). Figures 4g, 4h, and 4i show soil available water of the third layer (30~50 cm). Figures 4j, 4k, and 4l show normalized soil moisture. Figures 4m, 4n, and 4o show the drought-stressed days. Soil available water is the difference between soil water content and wilting point). Normalized soil moisture is calculated by  $\omega = (\theta - \theta_{\min}) / (\theta_{\max} - \theta_{\min})$ , where,  $\theta$  is soil moisture,  $\theta_{\max}$  and  $\theta_{\min}$  are field capacity and wilting point, respectively.

[18] The 0.5 and 1.5 precipitation amount levels were obtained by multiplying respective 0.5 and 1.5 with precipitation amounts in each event in the ambient level. Thus the 3 precipitation amount levels were ambient (854.5 mm a<sup>-1</sup>, denoted as 1.0 P), halved (427 mm a<sup>-1</sup>, 0.5 P), and one and a half (1283 mm a<sup>-1</sup>, 1.5 P) (Figures 2a, 2c, and 2e). The 0.5 P and 1.5 P precipitation amounts at the high intensity precipitation level were obtained also by multiplying respective 0.5 and 1.5 with precipitation amounts in each event (Figures 2d and 2f). The mean temperature of 2002 was 15.4°C. The warming scenario was achieved by adding 2°C to daily temperatures. The control atmospheric CO<sub>2</sub> concentration ([CO<sub>2</sub>]) was assumed to be 360 ppm and the doubled atmospheric [CO<sub>2</sub>] was 720 ppm.

[19] The five levels of soil AWC were defined according to variations in soil texture and corresponding soil hydrological properties. Grasslands have diverse soil texture types. In central grassland region of U.S.A., the soil texture ranged from sand and sandy loam to silt loam and silt clay

loam. Soil water holding capacity among those soil types ranged from 0.062 to 0.33 g water g<sup>-1</sup> soil [Lane *et al.*, 1998]. We assigned five soil texture types to cover the whole range in nature. These soil texture types were sand, sandy loam, loam, silt loam, and clay loam with field capacities ranging from 10% to 45% (volumetric water content) and wilting point from 5% to 15% (Table 2). Accordingly, the available water capacities (AWC) for the five soil texture types were 5% (sand), 7.5% (sandy loam), 15% (silt loam), 23% (loam), and 30% (clay loam), which were five levels of AWC in this study. Since soil texture varied slightly with depth [Dodd and Lauenroth, 1997], all of the soil layers were assumed to have the same field capacity and wilting point for simplifying interpretation of modeling results. We applied the 90 scenarios to model simulations after the model was run 1200 years and reached an equilibrium state.

[20] Drought-stressed days in a year were used as an index to show the level of drought stress on plants. It was

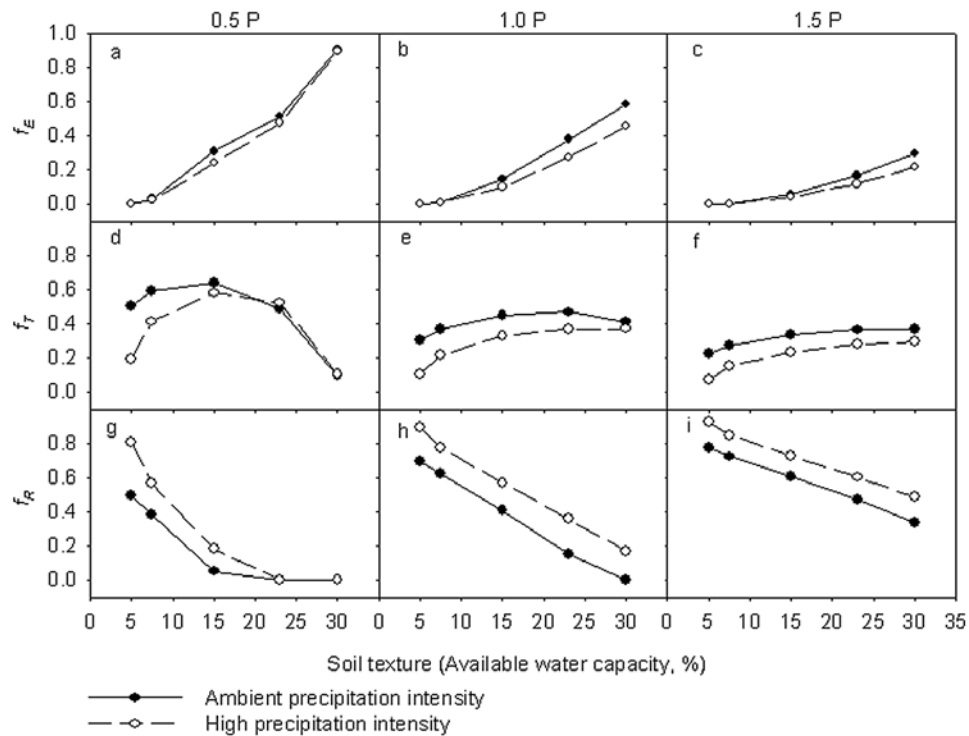


**Figure 5.** Proportions of water loss via Evaporation, Transpiration and Runoff.  $f_E$ : Evaporation/Precipitation;  $f_T$ : Transpiration/Precipitation;  $f_R$ : Runoff/Precipitation; E/ET: the ratio of evaporation to evapotranspiration.

defined as the number of days with normalized soil moisture below 0.3 in a year. Normalized soil moisture ( $\omega$ ) was defined by

$$\omega = \frac{W_{soil} - W_{min}}{W_{max} - W_{min}} \quad (3)$$

where,  $W_{max}$  was soil water holding capacity,  $W_{min}$  was wilting point,  $W_{soil}$  was soil moisture. In the TECO model, if  $\omega$  was below 0.3, photosynthesis and plant growth rate would be stressed.

### 3. Results

#### 3.1. Data: Model Comparison

[21] At equilibrium, the simulated soil carbon content was around  $8500 \text{ g}\cdot\text{m}^{-2}$ , which agreed with the measured soil carbon content well [Luo *et al.*, 2001]. The simulated litter was  $370 \text{ g}\cdot\text{m}^{-2}$ , which was very close to the measured value  $384 \pm 21 \text{ g}\cdot\text{m}^{-2}$ . The soil moisture, soil respiration, and aboveground biomass agreed with measurements well (Figure 3). Simulated soil moisture was correlated with the observed values by  $y = 0.72x + 6.6$ ,  $R^2 = 0.50$  ( $x$  was observation and  $y$  was simulation) with a mean absolute bias (ABS) 5.11 and a relative bias (RB)  $-2.5\%$ . Simulated soil moisture was slightly higher than the measured values when soil was very dry. Simulated and observed soil respirations had a regression equation  $y = 0.83x + 0.77$ ,  $R^2 = 0.57$ , and ABS was 0.82 and the RB was 17.6%. In winter, the simulated soil respiration was slightly higher than the measured values. The ABS between

simulated and observed aboveground biomass was 0.57 and RB was  $-3.4\%$  ( $y = 0.43x + 140.36$ ,  $R^2 = 0.57$ ).

#### 3.2. Ecosystem Responses to Changes in Precipitation With Different Soil Texture Types

[22] The annual mean soil available water (the difference between soil moisture and wilting point, %) increased with soil AWC under three precipitation scenarios (Figures 4a–4c). The soil available water in deep layers increased with AWC more than that in the surface layer. In the surface layer (0~10 cm), soil available water increased from 3% to 12% with soil AWC from 5% to 30% whereas it increased from 5% to 18% in the third layer (30~50 cm) at the ambient precipitation amount (1.0P) (Figures 4e and 4h). The same pattern occurred when precipitation increased by 50% (1.5 P) (Figures 4f and 4i) or decreased 50% (0.5 P) (Figures 4d and 4g). At 1.5 P, the annual mean soil available water was generally higher than that at 0.5 P or 1.0 P.

[23] The normalized soil moisture ( $\omega$  in equation (3)) showed different patterns with AWC at the three precipitation levels. At 1.0 P, it nearly kept a constant around 0.73 along soil AWC (Figure 4k). In contrast, it decreased from 0.70 to 0.56 at 0.5 P and increased from 0.71 to 0.81 at 1.5 P (Figures 4j and 4l). As a consequence, the drought-stressed days showed similar patterns. At 1.0 P, it was around 68~84 70 d along the soil AWC gradient from 5% to 30% (Figure 4n). At 0.5 P, the drought-stressed days increased from 60 d to 135 d with AWC (Figure 4m). At 1.5P, the drought-stressed days decreased from 82 d to 37 d (Figure 4o).

[24] Precipitation intensity influenced soil moisture along the gradient of soil AWC. At 1.0 P, the annual mean soil

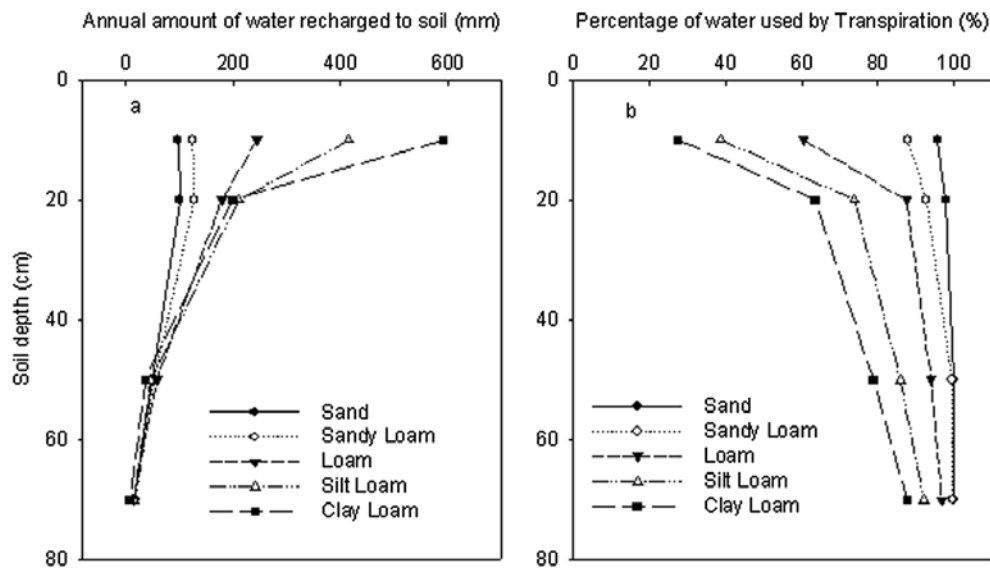


**Figure 6.** Water contributions to transpiration along soil depth by the five soil texture types. (a) The water recharged to soil layers every year, which is equal to the water used by evapotranspiration in these layers at equilibrium state. (b) The ratios of the water transpired through plants in every layer.

available water was lower at ambient than at high precipitation intensity when AWC was 30% (Figure 4b). At 0.5 P, high precipitation intensity led to higher annual mean soil moisture than that at ambient intensity (Figure 4a) and did not cause much difference at 1.5 P (Figure 4c). With all the three precipitation amount levels, high precipitation intensity resulted in lower water content in the surface layer but higher soil water content in the deep layer than the ambient

intensity regardless of soil textures except the deep layer at 1.5 P (Figures 4d–4i).

[25] Fractions of precipitation used for evaporation and transpiration increased generally with AWC but decreased for runoff (Figure 5). The fraction of precipitation used for evaporation increased continuously with AWC (Figures 5a–5c). The fraction of precipitation for transpiration increased with soil AWC at its low range and gradually leveled off at

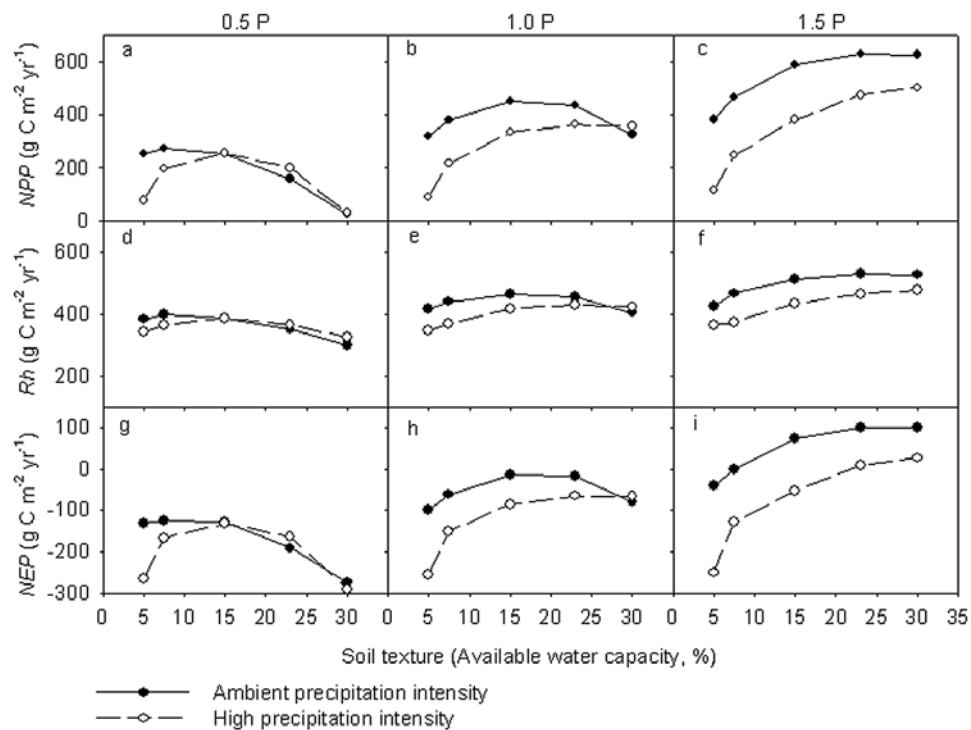


**Figure 7.** Soil texture effects on NPP,  $R_h$ , and NEP at three precipitation amount levels and two frequencies.

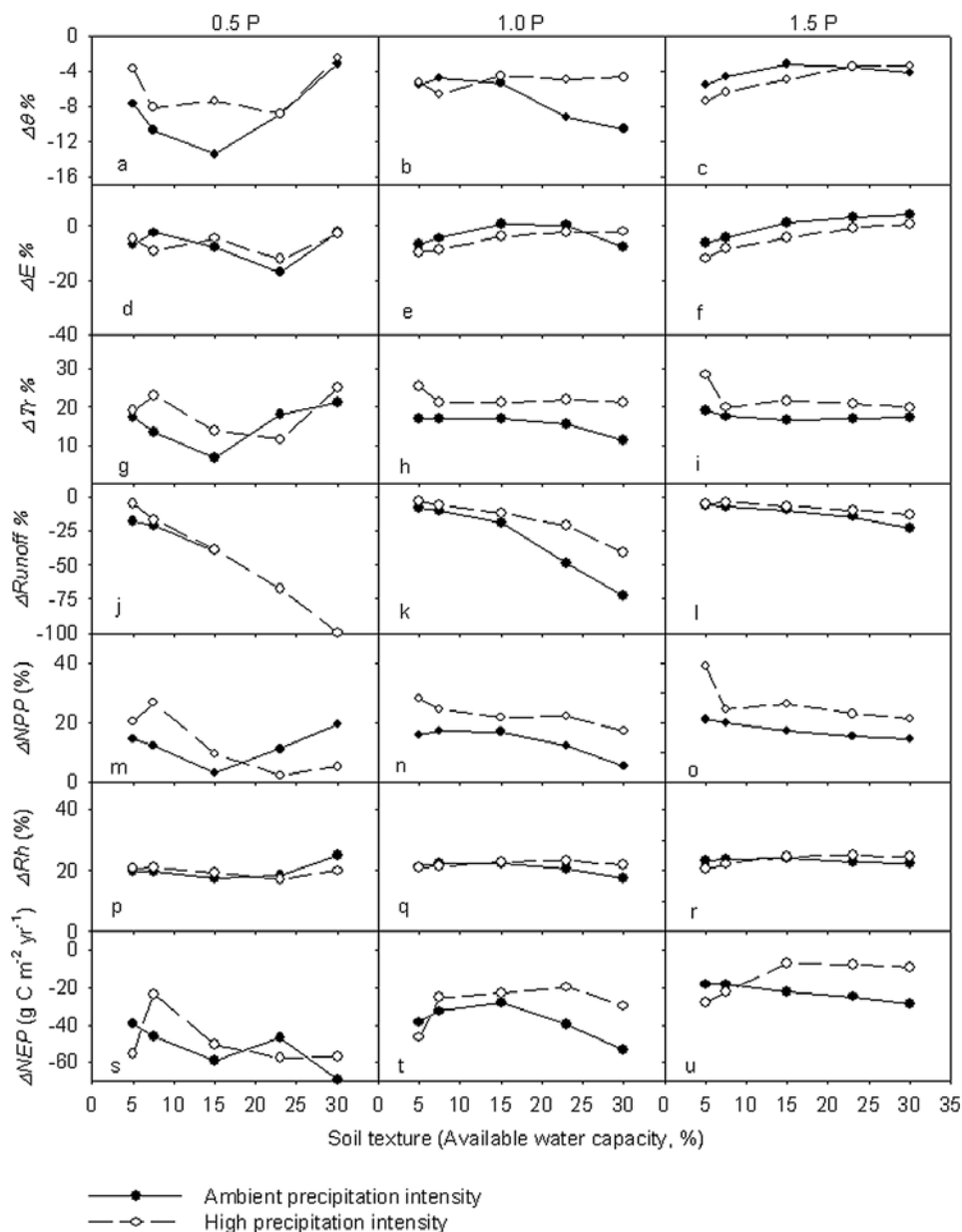


**Figure 8.** Effects of soil texture on grassland responses to warming (+2°C). The relative changes in soil water content, evaporation, transpiration, runoff, NPP, Rh, and NET with available water capacity is shown.  $\Delta\theta\%$ : percentage change in soil water content ( $\Delta\theta\% = (\theta_{2^\circ\text{C}} - \theta_{\text{amb.}}) / \theta_{\text{amb.}} \times 100$ ).  $\Delta E\%$ : percentage change in evaporation ( $\Delta E\% = (E_{2^\circ\text{C}} - E_{\text{amb.}}) / E_{\text{amb.}} \times 100$ ).  $\Delta \text{Tr}\%$ : percentage change in transpiration ( $\Delta \text{Tr}\% = (\text{Tr}_{2^\circ\text{C}} - \text{Tr}_{\text{amb.}}) / \text{Tr}_{\text{amb.}} \times 100$ ).  $\Delta \text{Runoff}\%$ : percentage change in runoff ( $\Delta \text{Runoff}\% = (\text{Runoff}_{2^\circ\text{C}} - \text{Runoff}_{\text{amb.}}) / \text{Runoff}_{\text{amb.}} \times 100$ ).  $\Delta \text{NPP}\%$ : percentage change in NPP ( $\Delta \text{NPP}\% = (\text{NPP}_{2^\circ\text{C}} - \text{NPP}_{\text{amb.}}) / \text{NPP}_{\text{amb.}} \times 100$ ).  $\Delta \text{Rh}\%$ : percentage change in  $R_h$  ( $\Delta \text{Rh}\% = (\text{Rh}_{2^\circ\text{C}} - \text{Rh}_{\text{amb.}}) / \text{Rh}_{\text{amb.}} \times 100$ ).  $\Delta \text{NEP}\%$ : percentage change in NEP ( $\Delta \text{NEP}\% = (\text{NEP}_{2^\circ\text{C}} - \text{NEP}_{\text{amb.}}) / \text{NEP}_{\text{amb.}} \times 100$ ).

its high range at 1.0 P and 1.5 P (Figures 5e and 5f). At 0.5 P, it first increased with AWC, reached a maximum at AWC of 15%, and then declined sharply (Figure 5d). The fraction of precipitation for runoff decreased with soil AWC continuously (Figures 5g–5i). At 0.5 P, it approached 0 at the 23% of AWC (Figure 5g). In general, high intensity of precipitation led to higher runoff, lower evaporation and transpiration than those at the ambient intensity with the three precipitation amounts.

[26] Variations in partitioning between transpiration and evaporation with AWC were also reflected in the vertical distribution of the water recharged to soil (Figure 6). Increases in AWC in loam soils resulted in increases in water that was recharged to the surface layer (Figure 6a). However, the ratio of the water in these layers used by transpiration decreased with AWC (Figure 6b).

[27] NPP,  $R_h$ , and NEP usually increased with AWC, especially with high precipitation amounts (Figure 7). At

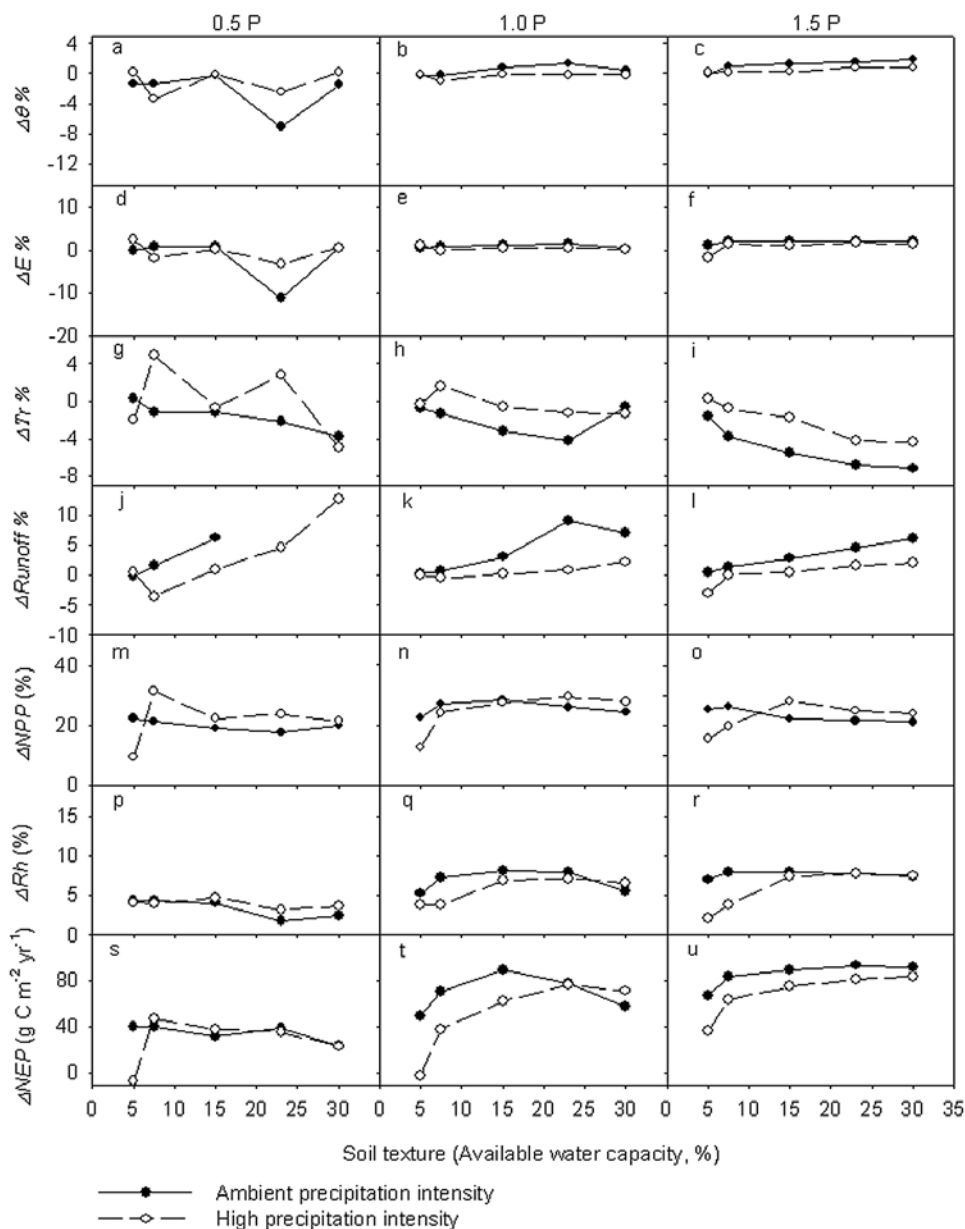


**Figure 9.** Effects of soil texture on grassland responses to elevated  $[CO_2]$ . The relative changes in soil water content, evaporation, transpiration, runoff, NPP,  $R_h$ , and NEP with soil available water capacity are shown.  $\Delta\theta\%$ : percentage change in soil water content ( $\Delta\theta\% = (\theta_{2CO_2} - \theta_{amb.}) / \theta_{amb.} \times 100$ ).  $\Delta E\%$ : percentage change in evaporation ( $\Delta E\% = (E_{2CO_2} - E_{amb.}) / E_{amb.} \times 100$ ).  $\Delta Tr\%$ : percentage change in transpiration ( $\Delta Tr\% = (Tr_{2CO_2} - Tr_{amb.}) / Tr_{amb.} \times 100$ ).  $\Delta Runoff\%$ : percentage change in runoff ( $\Delta Runoff\% = (Runoff_{2CO_2} - Runoff_{amb.}) / Runoff_{amb.} \times 100$ ).  $\Delta Runoff\%$ : percentage change in runoff ( $\Delta Runoff\% = (Runoff_{2CO_2} - Runoff_{amb.}) / Runoff_{amb.} \times 100$ ).  $\Delta NPP\%$ : percentage change in NPP ( $\Delta NPP\% = (NPP_{2CO_2} - NPP_{amb.}) / NPP_{amb.} \times 100$ ).  $\Delta Rh\%$ : percentage change in  $R_h$  ( $\Delta Rh\% = (Rh_{2CO_2} - Rh_{amb.}) / Rh_{amb.} \times 100$ ).  $\Delta NEP\%$ : percentage change in NEP ( $\Delta NEP\% = (NEP_{2CO_2} - NEP_{amb.}) / NEP_{amb.} \times 100$ ).

1.0 P, NPP,  $R_h$ , and NEP were the highest at soil AWC of 23% and lower at either low or high AWC (Figures 7b, 7e, and 7h). At 1.5 P, NPP,  $R_h$ , and NEP increased along the whole range of soil AWC (Figures 7c, 7f, and 7i). However, NPP,  $R_h$ , and NEP reached their peak points at AWC of 7.5% and then decreased with AWC at 0.5 P, (Figures 7a, 7b, and 7g). High precipitation intensity generally led to

lower NPP,  $R_h$ , and NEP than did the ambient intensity at 1.0 P and 1.5 P. At 0.5 P, NPP and  $R_h$  at high intensity were slightly higher at the high range of soil AWC than them at ambient intensity (Figures 7a and 7d). Differences in NPP,  $R_h$ , and NEP between ambient and high precipitation intensities were larger in coarse textured

soils with low AWC than fine textured soils with high AWC (Figure 7).

### 3.3. Ecosystem Responses to Warming With Different Soil Texture Types

[28] Our modeling results show that warming decreased soil moisture at all of the five soil texture types (Figures 8a–8c). The relative decreases in soil moisture became larger at 1.0 P along the gradient of soil AWC (Figure 8b). At 0.5 P, the largest relative decrease occurred at AWC of 15% (Figure 8a). At 0.5 P and 1.0 P, evaporation decreased under warming, especially at high soil AWC (Figures 8d and 8e). At 1.5 P, warming resulted in a decrease in evaporation at low AWC but an increase at high AWC (Figure 8f). Transpiration in warming treatment increased by 10~25% with the three precipitation amount levels (Figures 8g–8i). Warming resulted in decreases in runoff by up to almost 100% (Figures 8j–8l). The relative decrease of runoff was smaller at low AWC than high AWC with all of the three precipitation levels. High precipitation intensity usually lessened warming effects on ecohydrological processes than the ambient intensity (Figures 8a–8l).

[29] Warming usually resulted in increases in NPP and  $R_h$  but decreases in NEP (Figures 8m–8u). Warming-induced relative increases in NPP were generally higher at high precipitation amount and also varied with AWC (Figures 8m–8o).  $R_h$  increased by about 20% at all of the five soil texture types with the three precipitation amount levels (Figures 8p–8r). Relative decreases in NEP were greater at low than high precipitation amounts and least at AWC in the range of 7.5–15% at 1.0 P (Figure 8t). The high precipitation intensity led to higher relative increases in NPP but lower relative decreases in NEP in most cases than ambient intensity along the gradient of AWC (Figures 8m–8u).

### 3.4. Ecosystem Responses to Doubled Atmospheric [CO<sub>2</sub>] With Different Soil Texture Types

[30] Doubled [CO<sub>2</sub>] had relatively less effects on ecohydrological processes than the 2°C warming (Figure 9 versus Figure 8). At 1.0 P and 1.5 P, doubled [CO<sub>2</sub>] usually resulted in increases in soil moisture, evaporation, and runoff but decreases in transpiration in comparison to that under ambient [CO<sub>2</sub>] (Figures 9a–9l). The relative increases or decreases in ecohydrological processes at doubled [CO<sub>2</sub>] became larger at high AWC. At 0.5 P, changes in evaporation and transpiration showed no apparent trend with AWC, while soil moisture decreased slightly (Figure 9a) and runoff generally increased under elevated [CO<sub>2</sub>] with AWC (Figure 9j). High precipitation intensity led to less changes in soil moisture, evaporation, transpiration, and runoff under elevated [CO<sub>2</sub>] than ambient intensity at 1.0 P and 1.5 P.

[31] The relative increases in NPP,  $R_h$ , and NEP induced by elevated [CO<sub>2</sub>] were generally lower at low than high soil AWC at 1.0 P and 1.5 P (Figures 9m–9u). Doubled [CO<sub>2</sub>] usually increased NPP by 10–25% and  $R_h$  by 2–8%, leading to a substantial increase in NEP. CO<sub>2</sub>-induced changes in NPP,  $R_h$ , and NEP at 0.5 P were less than at 1.0 P and 1.5 P (Figures 9m, 9p, and 9s). Generally, CO<sub>2</sub> effects on NPP,  $R_h$ , and NEP were higher with high than

ambient precipitation intensity at high AWC but lower at low soil AWC.

## 4. Discussion

### 4.1. Water Partitioning Among Runoff, Evaporation, and Transpiration

[32] Partitioning of precipitation among, runoff, evaporation, and transpiration is influenced by many factors, such as vegetation density, rooting depth, soil texture, and precipitation intensity and amounts. Our results showed that runoff decreased and evaporation increased with AWC (Figure 5) along the soil texture gradient from sand to clay loam (Table 2). Transpiration increased with AWC quickly in the low range and leveled off in the high range of AWC (Figure 5). The results are consistent with a notion in the literature [Noy-Meir, 1973; McAuliffe, 2003] that soil texture can strongly regulate the partitioning of precipitation water among runoff, evaporation, and transpiration by changing soil water storage and vertical distributions.

[33] Water partitioning between evaporation (E) and transpiration (T) has been an important issue in ecohydrological studies [Lauenroth and Bradford, 2006]. A few empirical studies have also partitioned evapotranspiration (ET) into E and T in semiarid shrublands over limited time periods. An isotope experiment conducted in a shortgrass steppe in semiarid northeastern Colorado showed that the proportion of water lost by evaporation (E/ET) during the growing season ranged from nil to about 40% [Ferretti *et al.*, 2003]. Another experiment conducted at a semiarid shrubland site in Chihuahuan Desert by sap-flow and Bowen ratio techniques showed that the total T/ET was 58% in growing season, but it was around 70% in August to October when the shrubs were not dormant [Scott *et al.*, 2006]. Reynolds *et al.* [2000] proposed that the T/ET varied from 7% to 80% at a warm desert site in a modeling study. A simulation study suggested that transpiration is a dominant component (53%) of the global terrestrial water vapor flux from the continents and may reach a maximum of 75% in densely vegetated regions [Choudhury *et al.*, 1998]. Our simulation showed that T/ET differed substantially among various soil types. A fine textured soil stores a large portion of water in upper layers (Figure 6a), favoring evaporative water loss from soil surface. In coarse textured soils, however, rapid dehydration of the surface soil layer results in low evaporation and saving water in deep layers for plant transpiration (Figure 6b) [Wythers *et al.*, 1999].

[34] The changes in water partitioning patterns with soil AWC also lead to changes in ecosystem productivity. As shown by our results, NEP and NPP decreased with AWC at halved precipitation amount, which paralleled with decreases in normalized soil moisture with AWC and increases in drought-stressed days with AWC. However, at high precipitation level (i.e., 1.5 P), NPP increased with AWC while normalized soil moisture increased and drought-stressed days decreased with AWC. Our simulations agreed with the inverse texture hypothesis [Noy-Meir, 1973] that net primary productivity was higher on coarse-textured soils than that on fine-textured soils at 0.5 P; the reverse was predicted at 1.5 P. Field data measured in the Central Grassland Region of the United States also showed similar patterns with

changes in soil texture [Sala *et al.*, 1988; Epstein *et al.*, 1997; Lane *et al.*, 1998].

#### 4.2. Soil Texture and Effects of Precipitation Intensity on Ecosystem

[35] Increases in precipitation intensity with decreased frequency have been projected as a possible scenario of climate change in the future [Easterling *et al.*, 2000]. Field experiments showed that extreme rainfall events, without concurrent changes in water amounts could lead to increases in temporal variability in soil moisture [Knapp *et al.*, 2002; Fay *et al.*, 2003]. Carbon cycling processes, such as photosynthesis, above ground net primary productivity (ANPP) [Fay *et al.*, 2003; Knapp *et al.*, 2002], and soil respiration [Harper *et al.*, 2005], were also reduced because of high soil moisture variability.

[36] Our modeling results showed that high precipitation intensity led to more drought-stressed days than the ambient intensity in most cases (Figures 4m–4o), which was consistent with field experimental results. Furthermore, the modeling results enriched experimental results in the work of Knapp *et al.* [2002] by circumscribing conditions under which increased precipitation intensity with reduced frequency led to either decreases or increases in ecosystem production. High precipitation intensity with the same precipitation amount usually led to high drought stress and low NPP as shown by Knapp *et al.* [2002]. However, if precipitation amount was low (0.5P), for example, the high precipitation intensity could lead to higher soil moisture and less drought-stressed days than the ambient intensity when AWC was 15% or higher. At 1.0 P, the high precipitation intensity also decreased drought-stressed days when AWC was 30%, (Figure 4). That was because the fine textured soils stored rainwater from large precipitation events with high field capacity. Additionally, more water was stored in deep soil layers at high precipitation intensity than that at the ambient intensity. As a result, runoff and evaporation decreased, and water that was available to plants increased.

[37] Increases in soil moisture and decreases of drought-stressed days resulted in increase in NPP. As shown by the simulations, when precipitation amount was low (0.5 P) and soil AWC was high, NPP at high precipitation intensity was higher than at ambient precipitation intensity. However, with increases in precipitation amount (e.g., 1.5 P), high precipitation intensity led to lower NPP than ambient intensity. These results indicate that soil texture can strongly regulate effects of precipitation intensity on soil moisture content and ecosystem carbon processes.

#### 4.3. Soil Texture and Ecosystem Responses to Warming and Elevated [CO<sub>2</sub>]

[38] Both warming and elevated CO<sub>2</sub> can alter plant production through their direct influences on plant physiology and their indirect influences mediated by changes in soil water content [Shaver *et al.*, 2000; Morgan *et al.*, 2004; Parton *et al.*, 2007]. Experimental studies have shown that the indirect effects induced by changes in soil moisture play a critical role in regulating ecosystem responses to warming and elevated [CO<sub>2</sub>] [Nowak *et al.*, 2004; Volk *et al.*, 2000; Wullschlegel *et al.*, 2002; Morgan *et al.*, 2004]. As a result, the factors that affect soil water dynamics (e.g., soil AWC)

can regulate ecosystem responses to warming and elevated CO<sub>2</sub>.

[39] Warming-induced decreases in soil moisture usually aggravate drought stress on ecosystems [Harte *et al.*, 1995; Saleska *et al.*, 1999; Wan *et al.*, 2002]. Although warming usually stimulates plant growth productivity in most field studies [Rustad *et al.*, 2001], NPP may decrease if the negative effects of warming-induced soil drought override warming stimulation on plant growth [Saleska *et al.*, 1999]. Experimental results have shown that warming improved plant growth in spring and fall but limited it in summer because of drought stress induced by warming treatment [Wan *et al.*, 2005]. Soil texture can tip off a balance between the negative and the positive effects of warming by regulating water partitioning among runoff, evaporation, and transpiration. Our simulation showed that the percentage of warming-induced increases in NPP diminished with AWC when temperature increased by 2°C degrees (Figures 8m–8o), especially at 0.5 P. NEP has a substantial decrease in warming treatments because that warming induced increases in respiratory C releases were larger than the increases in C uptake.

[40] In contrast to the warming effects on soil moisture, elevated atmospheric [CO<sub>2</sub>] usually results in increases in soil moisture by decreasing stomatal conductance of many plant species [Morgan *et al.*, 2004]. Field experiments also showed that increased water consumption from increased primary productivity under elevated [CO<sub>2</sub>] offset the decreased water loss from reduced stomatal conductance [Nowak *et al.*, 2004]. Consequently, soil water content was hardly changed. Our simulation didn't show many changes in soil moisture along AWC gradient either.

[41] Along the soil AWC gradient from 5% to 30%, the increases in NPP varied from 5% to 30% (Figures 8m–8o) induced by warming and from 10% to 30% by doubled [CO<sub>2</sub>] (Figures 9m–9o). The simulation results indicate that soil texture can substantially affect ecosystem responses to warming and elevated [CO<sub>2</sub>]. The sites where warming and/or CO<sub>2</sub> experiments were conducted have varied soil texture types and different soil hydrological properties [Rustad *et al.*, 2001; Morgan *et al.*, 2004]. Variations in soil texture with changes in soil water availability may play a role in diverse responses of ecosystem production to experimental warming and elevated atmospheric [CO<sub>2</sub>].

## 5. Conclusion

[42] The modeling results showed that soil hydrological properties can modify ecosystem responses to changes in precipitation patterns, warming, and elevated atmospheric [CO<sub>2</sub>] by altering partitioning of rainwater among runoff, evaporation, and transpiration. Water partitioning patterns along a soil texture gradient alter soil water content, and then regulate ecosystem responses to changes in global change factors indirectly. Our simulation showed that NPP, R<sub>h</sub>, and NEP usually increased with soil AWC. Such increases were amplified by precipitation amounts. Warming-induced increases in NPP diminished with soil AWC, whereas warming effects on R<sub>h</sub> did not vary much in different soil texture types. Stimulation of NPP, R<sub>h</sub>, and NEP by elevated [CO<sub>2</sub>] was usually lower in coarse than fine textured soils. Considering high variations in soil

texture at field sites where experiments were conducted, hydrological properties of soil can be one of the major causes underlying variable responses of ecosystems to global change observed in field experiments. Therefore it is highly desirable to examine soil hydrological properties in regulating ecosystem responses to global change in future research.

## Appendix A: Model Description

[43] Terrestrial ECOlogical model (TECO) evolves from a terrestrial carbon sequestration (TCS) model [Luo and Reynolds, 1999] and is designed to examine ecosystem responses to perturbations in global change factors. TECO has four major components: canopy photosynthesis, soil water dynamic, plant growth (allocation and phenology), soil carbon transfers (Figure 1) The photosynthesis and soil moisture dynamics are simulated at hourly time step while the plant growth and the carbon transfer are simulated at daily step.

### A1. Canopy Photosynthesis Submodel

[44] Canopy photosynthesis submodel is from a two-leaf photosynthesis model, which simulates canopy conductance, photosynthesis, transpiration, and energy partitioning [Wang and Leuning, 1998]. It consists of two parts: (1) a radiation model which calculates photosynthesis active radiation (PAR), near infrared radiation (NIR), and thermal radiation absorbed by sunlit and shaded leaves and (2) a coupled model of stomatal conductance, photosynthesis and transpiration.

#### A1.1. Coupled Model of Stomata-Photosynthesis-Transpiration

[45] The coupled model of stomatal conductance, photosynthesis and transpiration for the big sunlit leaf ( $i = 1$ ) or big shaded leaf ( $i = 2$ ) is given by the following equations. Energy balance

$$Q_{n,i} = \lambda E_{c,i} + H_{c,i} \quad (A1)$$

Transpiration

$$E_{c,i} = G_{s,i} D_{s,i} = G_{w,i} (D_a + s \Delta T_i) \quad (A2)$$

Sensible heat

$$H_{c,i} = G_{h,i} c_p \Delta T_i \quad (A3)$$

Photosynthesis-gas diffusion

$$A_{c,i} = b_{sc} G_{s,i} (C_{s,i} - C_i) = G_{c,i} (C_a - C_i) \quad (A4)$$

Stomatal conductance

$$G_{s,i} = G_{0,i} + \frac{a_1 f_w S_{NSC} A_{c,i}}{(C_{s,i} - \Gamma)(1 + D_{s,i}/D_0)} \quad (A5)$$

Photosynthesis-biochemistry

$$A_{c,i} = V_{n,i} - R_{d,i} \quad (A6)$$

where,  $Q_{n,i}$  is net available energy,  $E_{c,i}$  is transpiration,  $H_{c,i}$  is sensible heat,  $\lambda$  is latent heat of vaporization for water.  $D_a$

and  $D_{s,i}$  are saturated deficit of water vapor pressure (VPD) in ambient air and at leaf surface, respectively.  $G_{s,i}$  is stomatal conductance of a leaf or big leaf for  $H_2O$ ,  $G_{0,i}$  is stomatal conductance of a leaf or big leaf for  $H_2O$  when net leaf photosynthesis is zero.  $G_{w,i}$  and  $G_{c,i}$  are total conductance from the intercellular space of the leaves to the reference height above the canopy for  $H_2O$  and  $CO_2$ , respectively.  $G_{h,i}$  is the total conductance for the heat transfer from leaf surface to reference height above the canopy,  $c_p$  is specific heat of the air,  $\Delta T_i$  is the temperature difference between the surface of the big leaf and that of the air at the reference height,  $s$  is the slope of the function relating saturated water vapor *mol* fraction to temperature and  $b_{sc}$  is the ratio of diffusivity of  $CO_2$  and  $H_2O$  through the stomata.  $A_{c,i}$  is the net photosynthesis rate,  $V_{n,i}$  is the net carboxylation rate,  $R_{d,i}$  is the day respiration rate.  $C_a$ ,  $C_{s,i}$  and  $C_i$  are  $CO_2$  *mol* fractions in the air, at the leaf surface, and intercellular spaces, respectively.  $\Gamma$  is  $CO_2$  compensation point of leaf photosynthesis,  $D_0$  is a parameter for stomatal sensitivity to VPD.  $a_1$  is an experience constant, which is related to the intercellular  $CO_2$  concentration by  $C_i/C_{s,i} = 1 - 1/a_1$ .  $f_w$  is soil moisture scaling factor, and  $S_{NSC}$  is a scaling factor derived by the size of nonstructural pool. Equation (A6) is a biochemical model of photosynthesis which is used to calculate biochemical processes limited photosynthesis rate. More details are by Farquhar *et al.* [1980] and Wang and Leuning [1998].

#### A1.2. Radiation Absorption

[46] The net energy available to the big leaf  $i$  in wave band  $j$ ,  $Q_{n,i}$ , is calculated as:

$$Q_{n,i} = \sum_{j=1}^3 Q_{i,j} \quad (A7)$$

[47] Leaf temperature should be known for calculating absorbed long-wave radiation ( $Q_{i,3}$ ). However, it can be skipped by using the isothermal net radiation ( $Q_{n,i}^*$ ).

$$Q_{n,i}^* = Q_{n,i} + c_p G_{r,i} \Delta T_i \quad (A8)$$

[48] Loss of thermal radiation of the big leaf to the air under nonisothermal conditions is calculated by  $G_{r,i} [= 4\epsilon_f \sigma T_a^3/c_p]$ , where,  $\epsilon_f$  is the leaf emissivity,  $\sigma$  is the Steffan Boltzman constant and  $T_a$  is air temperature ( $K$ ).

### A2. Soil Water Dynamics Submodel

[49] Soil is stratified into 10 layers (the thickness of the first layer is 10 cm, all others are 20 cm). Infiltration adds water to soil layers in a cascading fashion according to soil hydrologic properties. When the ten layers of soil is filled, excessive water runs off. Evaporation is calculated by the evaporation equation in the SiB2 [Sellers *et al.*, 1996]. The allocation of evaporation in the ten soil layers follows the ALFALFA model [Luo *et al.*, 1995; Denison and Loomis, 1989]. The water transpired by plants is partitioned among the soil layers according to the fractions of roots in these layers. Soil water content is calculated as the budget between input

(precipitation and infiltration) and output (runoff, evaporation, and transpiration).

### A2.1. Infiltration

[50] Water flows to the next layer when the upper layer is filled. The depth to which water from a rainfall event can penetrate depends on precipitation amount, field capacity, and current soil water content. The model iterates the water content of each soil layer after calculating evaporation, and transpiration.

### A2.2. Transpiration

[51] Transpiration is calculated in the canopy model by stomatal conductance and the relative humidity difference between inside and outside of the leaves. The water contribution to transpiration of every soil layers is calculated according to the fractions of roots in these soil layers.

### A2.3. Evaporation

[52] Soil surface evaporation is calculated by the following equation [Sellers *et al.*, 1996]:

$$E_s = \frac{e^*(T_{soil}) - e_a}{r_{soil} + r_d} \frac{\rho c_p}{\gamma} \frac{1}{\lambda} \quad (A9)$$

where  $E_s$  is soil evaporation,  $e^*(T_{soil})$  is the saturation vapor pressure at the temperature of the soil,  $e_a$  is the atmospheric vapor pressure,  $r_{soil}$  is a soil resistance term,  $r_d$  is the aerodynamic resistance between the ground and the canopy air space,  $\rho$  is the density of air,  $c_p$  is the specific heat of air,  $\gamma$  is the psychrometric constant,  $\lambda$  is the latent heat of sublimation [Sellers *et al.*, 1996].

### A2.4. Runoff

[53] If soil water content is greater than soil water holding capacity, then runoff occurs

$$\begin{aligned} \text{Runoff} &= W_{soil} - W_{max} \\ \text{then, } W_{soil} &= W_{max} \end{aligned} \quad (A10)$$

where,  $W_{max}$  is soil water holding capacity,  $W_{min}$  is soil water content (v/v %).

### A2.5. Soil Water Content

[54] Soil water content is updated hourly according to the budget between precipitation and evapotranspiration.

$$W_{soil} = W_{soil0} + P - ET \quad (A11)$$

where,  $ET$  is evapotranspiration.

### A2.6. Soil Moisture Scalar

[55] A soil moisture scalar is used to regulate photosynthesis rate, plant growth rate, and soil carbon turnover time. It is calculated by the following equation.

$$f_w = \min\left(1.0, 3.33 \cdot \left(\frac{W_{soil} - W_{min}}{W_{max} - W_{min}}\right)\right) \quad (A12)$$

where,  $W_{min}$  is wilting point.

## A3. Plant Growth Submodel

[56] The plant growth submodel simulates the processes of carbon allocation to leaves, stems, and roots (i.e., plant growth), and the production of litter fall. The model has six carbon pools: one nonstructural carbon pool (NSC), one leaf

carbon pool ( $Q_L$ ), one stem carbon pool ( $Q_W$ ), and three root carbon pools ( $Q_{R1}$ ,  $Q_{R2}$ ,  $Q_{R3}$ ). The carbon fixed by photosynthesis enters into NSC first. And then, the carbon in NSC is used by autotrophic respiration or allocated to plant tissues via plant growth. The carbon allocation from NSC to the five plant C-pools is determined by their growth rates. Phenology is presented in the processes of leaf growing and falling with changes in leaf area index.

### A3.1. Autotrophic Respiration

[57] Autotrophic respiration ( $R_a$ ) is calculated at daily step based on temperature (either air or soil temperatures, for above and below ground tissues, respectively), tissue biomass, and phenology by Arrhenius equation [Ryan, 1991; Lloyd and Taylor, 1994].

$$R_i = R_{i0} \cdot e^{a \cdot T} \quad (A13)$$

where,  $R_{i0} = b \cdot BM$ ,  $T$  is temperature of air or soil,  $a$  and  $b$  are constants,  $BM$  is biomass.

### A3.2. Plant Growth Rate

[58] It follows the idea from the ALFALFA model [Denison and Loomis, 1989; Luo *et al.*, 1995], which simulate plant growth rate by root/shoot ratio, scalar of NSC, and a scalar of leaf area index.

$$G_i = G_{max_i} \cdot BM_i \cdot S_{r/s} \cdot S_{nsc} \cdot S_{LAI} \quad (A14)$$

where,  $i$  = leaf, stem, or root.  $G_i$  is the growth rate,  $G_{max_i}$  is the maximum relative growth rate,  $BM_i$  is the biomass of leaves, stems or roots.  $S_{r/s}$ ,  $S_{nsc}$  and  $S_{LAI}$  are the scaling factors derived from root/shoot ratio, the size of nonstructural carbon pool, and leaf area index, respectively.

### A3.3. Litter Production

[59] Leaf fall and root turnover is induced by soil drought and low air temperature in the autumn following the approach of Arora and Boer [2005]. Stem fall is only controlled by its intrinsic turnover rate.

$$\begin{aligned} \gamma_T &= \gamma_{T_{max}} (1 - \beta_T)^{br} \\ \gamma_W &= \gamma_{W_{max}} (1 - W)^{bw} \end{aligned} \quad (A15)$$

where,  $\gamma_{T_{max}}$  and  $\gamma_{W_{max}}$  are maximum rates of leaf fall induced by low temperature and drought respectively.  $\beta_T$  and  $W$  are scaling factors controlling the rate of leaf fall. Then, leaf senescence ( $D_L$ ), woody turnover ( $D_S$ ) and root turnover ( $D_R$ ) are computed by the following equation.

$$\begin{aligned} D_L &= q_L (\gamma_T + \gamma_W) \\ D_S &= q_W / \tau_W \\ D_R &= q_R (\gamma_T + \gamma_W) \end{aligned} \quad (A16)$$

where,  $q_L$ ,  $q_W$  and  $q_R$  are the C-pool sizes of leaves, stems, and roots, respectively.  $\tau_W$  is turnover time of carbon in stem C-pool.

### A3.4. Phenology

[60] Phenology is represented by periodical variations of leaf area index (LAI) and switches between dormant state and growing state. In winter, grasses remain in dormant state until the arrival of favorable weather conditions in spring. The growing state is initiated by a certain level of growing degree days above 5°C (GDD<sub>5</sub>). In the first several

days of a growing season, leaf growth consumes the carbon stored in nonstructural carbon pool (NSC). After the stored carbon is used up, leaf growth is based on the carbon from photosynthesis. LAI is controlled by the budget of leaf growth and senescence. If leaf growth overrides leaf senescence, LAI increases, and vice versa. In the fall, the onset of dormant state is initiated when LAI meets a minimum value (<0.1).

#### A4. Carbon Transfer Submodel

[61] The carbon transfer submodel is evolved from TCS [Luo and Reynolds, 1999] and VAST [Barret, 2002]. It is used to simulate the carbon flow from plant tissues to litters and soils, and then to atmosphere. There are five carbon pools in the carbon transfer submodel, which are fine litters ( $Q_F$ ), coarse litters ( $Q_C$ ), and three soil carbon pools defined by three soil layers ( $Q_{S1}$ ,  $Q_{S2}$ ,  $Q_{S3}$ ) (Figure 1). The carbon that is allocated to leaves ( $Q_F$ ), stems ( $Q_W$ ), and roots ( $Q_{R1}$ ,  $Q_{R2}$ ,  $Q_{R3}$ ) flows through these C-pools, and then returns to atmosphere as  $\text{CO}_2$ .

[62] The turnover time of carbon in leaf C-pool ( $\tau_L$ ) is determined by the growth and fall of leaves. The turnover times of carbon in stem C-pool ( $\tau_W$ ) and root C-pool ( $\tau_{R1}$ ,  $\tau_{R2}$ ,  $\tau_{R3}$ ) are assumed to be constants. The turnover times of carbon in fine litter ( $\tau_F$ ), coarse litter ( $\tau_C$ ), and soil carbon pools ( $\tau_{S1}$ ,  $\tau_{S2}$ ,  $\tau_{S3}$ ) are given by the following equation:

$$\tau_k = \tau_k^* / S_T \cdot S_\omega \quad (\text{A17})$$

where,  $\tau_k^*$  is the moisture and temperature independent turnover time,  $S_T$  and  $S_\omega$  are scalars of the moisture and temperature, which modify residence times of the carbon pools. The dynamics of  $k$ th C-pool,  $dq_k/dt$  ( $\text{gC m}^{-2} \cdot \text{d}^{-1}$ ), is calculated by equation (A18).

$$dq_k/dt = I_k - q_k/\tau_k \quad (\text{A18})$$

where,  $I_k$  is the input flux of carbon from upstream C-pools,  $q_k$  is the size of  $k$ th C-pool,  $\tau_k$  is the turnover time (days) of carbon in the  $k$ th C-pool,  $q_k/\tau_k$  is the daily carbon out flux of the  $k$ th pool. The daily carbon influx of the  $k$ th pool ( $I_k$ ) is given by:

$$\begin{aligned} I_F &= L_{Fall} + \eta_C W_{Fall} \\ I_C &= W_{Fall}(1 - \eta_C) \\ I_{S1} &= q_{R1}/\tau_{R1} + q_F/\tau_F \theta_F + q_C/\tau_C \theta_C \\ I_{S2} &= q_{R2}/\tau_{R2} + q_{S1}/\tau_{S1} \theta_{S1} \\ I_{S3} &= q_{R3}/\tau_{R3} + q_{S2}/\tau_{S2} \theta_{S2} \end{aligned} \quad (\text{A19})$$

where,  $q_k$  is the size of the  $k$ th C-pool,  $\eta_C$  is the fragmentation coefficient of wood going to fine litter,  $\tau_k$  is the turnover time of the carbon in the  $k$ th C-pool, and  $\theta_k$  is the partitioning parameter of C-pools. Heterotrophic respiration from litter and soil carbon pools is given by the following equation:

$$R_{hk} = \sum q_k/\tau_k \cdot f_k' \quad (\text{A20})$$

where,  $f_k'$  is the fraction of carbon out flux released to the atmosphere as  $\text{CO}_2$  from the  $k$ th pool, which is given by:

$$\begin{aligned} f_F' &= 1 - \theta_F \\ f_C' &= 1 - \theta_C \\ f_{S1}' &= 1 - \theta_{S1} \\ f_{S2}' &= 1 - \theta_{S2} \\ f_{S3}' &= 1 \end{aligned} \quad (\text{A21})$$

[63] **Acknowledgments.** We thank Xuhui Zhou and Rebecca Sherry for providing measured soil respiration, biomass, and soil moisture data and Yingping Wang for providing the source code of the photosynthesis model. This study was financially supported by the U.S. National Science Foundation under DEB0078325, DEB 0444518, and DEB 0743778, and by the Office of Science (BER), Department of Energy, grants DE-FG03-99ER62800 and DE-FG02-06ER64319 and TERACC initiative (Terrestrial Ecosystem Responses to Atmospheric and Climatic Change, a research coordination network supported by the U.S. National Science Foundation under DEB 0090238).

#### References

- Arora, V. K., and G. J. Boer (2005), A parameterization of leaf phenology for the terrestrial ecosystem component of climate models, *Global Change Biol.*, *11*, 39–59.
- Ball, J. T., I. E. Woodrow, and J. A. Berry (1987), A model predicting stomatal conductance and its contribution to the control of photosynthesis under different environmental conditions, in *Progress in Photosynthesis Research*, edited by J. Biggens, pp. 221–224, Martinus Nijhoff, Zoetermeer, Netherlands.
- Barrett, D. J. (2002), Steady state turnover time of carbon in the Australian terrestrial biosphere, *Global Biogeochem. Cycles*, *16*(4), 1108, doi:10.1029/2002GB001860.
- Buckman, H. O., and N. C. Brady (1960), *The Nature and Properties of Soils*, Macmillan, New York.
- Choudhury, B. J., N. E. DiGrolamob, J. Susskindc, W. L. Darnell, S. K. Guptae, and G. Asrar (1998), A biophysical process-based estimate of global land surface evaporation using satellite and ancillary data. part II: Regional and global patterns of seasonal and annual variations, *J. Hydrol.*, *205*, 186–204.
- Denison, F., and B. Loomis (1989), *An Integrative Physiological Model of Alfalfa Growth and Development*, UC ANR Publication 1926, Univ. California, Davis.
- Dodd, M. B., and W. K. Lauenroth (1997), The influence of soil texture on the soil water dynamics and vegetation structure of a shortgrass steppe ecosystem, *Plant Ecol.*, *133*, 13–28.
- Easterling, D. R., G. A. Meehl, C. Parmesan, S. A. Changnon, T. R. Kar, and L. O. Mearns (2000), Climate extremes: Observations, modeling, and impacts, *Science*, *289*, 2068–2073.
- Epstein, H. E., W. K. Lauenroth, and I. C. Burke (1997), Effects of temperature and soil texture on ANPP in the Great Plains, U.S., *Ecology*, *78*, 2628–2631.
- Farquhar, G. D., S. von Caemmerer, and J. A. Berry (1980), A biochemical model of photosynthetic  $\text{CO}_2$  assimilation in leaves of  $\text{C}_3$  species, *Planta*, *149*, 78–90.
- Fay, P. A., J. D. Carlisle, A. K. Knapp, J. M. Blair, and S. L. Collins (2003), Productivity responses to altered rainfall patterns in a  $\text{C}_4$ -dominated grassland, *Oecologia*, *137*, 245–251.
- Ferretti, D. F., E. Pendall, J. A. Morgan, J. A. Nelson, D. LeCain, and A. R. Mosier (2003), Partitioning evapotranspiration fluxes from a Colorado grassland using stable isotopes: Seasonal variation and ecosystem implications of elevated atmospheric  $\text{CO}_2$ , *Plant Soil*, *254*, 291–303.
- Hanson, P. J., et al. (2004), Oak forest carbon and water simulations: Model intercomparisons and evaluations against independent data, *Ecol. Monogr.*, *74*, 443–489.
- Harper, C. W., J. M. Blair, P. A. Fay, A. K. Knapp, and J. D. Carlisle (2005), Increased rainfall variability and reduced rainfall amount decreases soil  $\text{CO}_2$  flux in a grassland ecosystem, *Global Change Biol.*, *11*, 322–334.
- Harte, J., M. S. Torn, F. R. Chang, B. Feifarek, A. P. Kinzig, R. Shaw, and K. Shen (1995), Global warming and soil microclimate: Results from a meadow-warming experiment, *Ecol. Appl.*, *5*, 132–150.
- IPCC (2001), *Climate Change 2001: The Scientific Basis. Contribution of Working Group I to the Third Assessment Report of the Intergovernmen-*

- tal Panel on Climate Change, edited by J. T. Houghton et al., Cambridge Univ. Press, New York.
- Jackson, R. B., J. Canadell, J. R. Ehleringer, H. A. Mooney, O. E. Sala, and E. D. Schulze (1996), A global analysis of root distributions for terrestrial biomes, *Oecologia*, *108*, 389–411.
- Jastrow, J. D., R. M. Miller, R. Matamala, R. J. Norby, T. W. Boutton, C. W. Rice, and C. E. Owensby (2005), Elevated atmospheric carbon dioxide increases soil carbon, *Global Change Biol.*, *11*, 2057–2064.
- Knapp, A. K., E. P. Hamerlynck, and C. E. Owensby (1993), Photosynthetic and water relations responses to elevated CO<sub>2</sub> in the C<sub>4</sub> grass *Andropogon gerardii*, *Int. J. Plant Sci.*, *154*, 459–466.
- Knapp, A. K., A. Fay, J. M. Blair, S. L. Collins, M. D. Smith, J. D. Carlisle, C. W. Harper, B. T. Danner, M. S. Lett, and J. K. McCarron (2002), Rainfall variability, carbon cycling, and plant species diversity in a mesic grassland, *Science*, *298*, 2202–2205.
- Körner, C., M. Diemer, B. Schöpfi, P. Niklaus, and J. Arnone (1997), The responses of alpine grassland to four seasons of CO<sub>2</sub> enrichment: A synthesis, *Acta Oecol.*, *18*, 165–175.
- Lane, D. R., D. P. Coffin, and W. K. Lauenroth (1998), Effects of soil texture and precipitation on above-ground net primary productivity and vegetation structure across the central grassland region of the United States, *J. Veg. Sci.*, *9*, 239–250.
- Lauenroth, W. K., and J. B. Bradford (2006), Ecohydrology and the partitioning AET between transpiration and evaporation in a semiarid steppe, *Ecosystems*, *9*, 756–767.
- Lloyd, J., and J. A. Taylor (1994), On the temperature dependence of soil respiration, *Funct. Ecol.*, *8*, 315–323.
- Luo, Y. (2007), Terrestrial carbon cycle feedback to climate warming, *Annu. Rev. Ecol. Evol. Syst.*, *38*, 683–712.
- Luo, Y., and J. F. Reynolds (1999), Validity of extrapolating field CO<sub>2</sub> experiments to predict carbon sequestration in natural ecosystems, *Ecology*, *80*, 1568–1583.
- Luo, Y., P. A. Meyerhoff, and R. S. Loomis (1995), Seasonal patterns and vertical distributions of fine roots of alfalfa (*Medicago sativa* L.), *Field Crops Res.*, *40*, 119–127.
- Luo, Y., D. Hui, and D. Zhang (2006), Elevated CO<sub>2</sub> stimulates net accumulations of carbon and nitrogen in land ecosystems: A meta-analysis, *Ecology*, *87*, 53–63.
- Luo, Y., S. Wan, D. Hui, and L. Wallace (2001), Acclimatization of soil respiration to warming in a tall grass prairie, *Nature*, *413*, 622–625.
- McAuliffe, J. R. (2003), The atmosphere-biosphere interface: the importance of soils in arid and semi-arid environments, in *Changing Precipitation Regimes and Terrestrial Ecosystems: A North America Perspective*, edited by J. F. Weltzin and G. R. McPherson, pp. 9–27, Univ. Arizona Press, Tucson.
- Miller, D. A., and R. A. White (1998), A conterminous United States multi-layer soil characteristics data set for regional climate and hydrology modeling, *Earth Interact.*, *2*, 1–26.
- Moore, L. A., and C. B. Field (2006), The effects of elevated atmospheric CO<sub>2</sub> on the amount and depth distribution of plant water uptake in a California annual grassland, *Global Change Biol.*, *12*, 578–587.
- Morgan, J. A., et al. (2004), Water relations in grassland and desert ecosystems exposed to elevated atmospheric CO<sub>2</sub>, *Oecologia*, *140*, 11–25.
- Niklaus, P. A., D. Spinnler, and C. Körner (1998), Soil moisture dynamics of calcareous grassland under elevated CO<sub>2</sub>, *Oecologia*, *117*, 201–208.
- Nippert, J. B., and A. K. Knapp (2007), Linking water uptake with rooting patterns in grassland species, *Oecologia*, *153*, 261–272.
- Nowak, R. S., S. F. Zitzer, D. Babcock, V. Smith-Longozo, T. N. Charlet, J. S. Coleman, J. R. Seemann, and S. D. Smith (2004), Elevated atmospheric CO<sub>2</sub> does not conserve soil water in the Mojave Desert, *Ecology*, *85*, 93–99.
- Noy-Meir, I. (1973), Desert ecosystems: Environment and producers, *Annu. Rev. Ecol. Evol. S.*, *4*, 25–51.
- Owensby, C. E., J. M. Ham, A. K. Knapp, and L. M. Auen (1999), Biomass production and species composition change in a tallgrass prairie ecosystem after long-term exposure to elevated atmospheric CO<sub>2</sub>, *Global Change Biol.*, *5*, 497–506.
- Parton, W. J., J. M. O. Scurlock, D. S. Ojima, D. S. Schimel, D. O. Hall, and SCOPEGRAM members (1995), Impact of climate change on grassland production and soil carbon worldwide, *Global Change Biol.*, *1*, 13–22.
- Parton, W. J., J. A. Morgan, G. Wang, and S. D. Grosso (2007), Projected ecosystem impact of the Prairie Heating and CO<sub>2</sub> Enrichment experiment, *New Phytol.*, *174*, 823–834.
- Reynolds, J. F., P. R. Kemp, and J. D. Tenhunen (2000), Effects of long-term rainfall variability on evapotranspiration and soil water distribution in the Chihuahuan Desert: A modeling analysis, *Plant Ecol.*, *150*, 145–159.
- Rodriguez-Iturbe, I., and A. Porporato (2004), *Ecohydrology of Water-Controlled Ecosystems: Soil Moisture and Plant Dynamics*, 442 pp., Cambridge Univ. Press, New York.
- Rosenbloom, N. A., S. C. Doney, and D. S. Schimel (2001), Geomorphic evolution of soil texture and organic matter in eroding landscapes, *Global Biogeochem. Cycles*, *15*, 365–382.
- Rustad, L. E., J. L. Campbell, G. M. Marion, R. J. Norby, M. J. Mitchell, A. E. Hartley, J. H. C. Cornelissen, J. Gurevitch, and GCTE-NEWS (2001), A meta-analysis of the response of soil respiration, net nitrogen mineralization, and aboveground plant growth to experimental ecosystem warming, *Oecologia*, *126*, 543–562.
- Ryan, M. G. (1991), Effects of climate change on plant respiration, *Ecol. Appl.*, *1*, 157–167.
- Sala, O. E., W. J. Parton, L. A. Joyce, and W. K. Lauenroth (1988), Primary production of the central grassland region of the United States, *Ecology*, *69*, 40–45.
- Saleska, S., J. Harte, and M. Torn (1999), The effect of experimental ecosystem warming on CO<sub>2</sub> fluxes in a montane meadow, *Global Change Biol.*, *5*, 125–141.
- Schulze, E. D., R. H. Robichaux, J. Grace, P. W. Rundel, and J. R. Ehleringer (1987), Plant water balance, *Bioscience*, *37*, 30–37.
- Scott, R. L., T. E. Huxman, W. L. Cable, and W. E. Emmerich (2006), Partitioning of evapotranspiration and its relation to carbon dioxide exchange in a Chihuahuan Desert shrubland, *Hydrol. Process.*, *20*, 3227–3243.
- Sellers, P. J., D. A. Randall, G. J. Collatz, J. A. Berry, C. B. Field, D. A. Dazlich, C. Zhang, G. D. Collelo, and L. Bounoua (1996), A revised land surface parameterization (SiB2) for atmospheric GCMs. part I: Model formulation, *J. Clim.*, *9*, 676–705.
- Shaver, G. R., et al. (2000), Global warming and terrestrial ecosystems: A conceptual framework for analysis, *BioScience*, *50*, 871–882.
- Singh, J. S., D. G. Milchunas, and W. K. Lauenroth (1998), Soil water dynamics and vegetation patterns in a semiarid grassland, *Plant Ecol.*, *134*, 77–89.
- Volk, M., A. Niklaus, and C. Körner (2000), Soil moisture effects determine CO<sub>2</sub> responses of grassland species, *Oecologia*, *125*, 380–388.
- Wan, S., Y. Luo, and L. L. Wallace (2002), Changes in microclimate induced by experimental warming and clipping in tallgrass prairie, *Global Change Biol.*, *8*, 754–768.
- Wan, S., D. Hui, L. L. Wallace, and Y. Luo (2005), Direct and indirect effects of experimental warming on ecosystem carbon processes in a tallgrass prairie, *Global Biogeochem. Cycles*, *19*, GB2014, doi:10.1029/2004GB002315.
- Wang, Y. P., and R. Leuning (1998), A two-leaf model for canopy conductance, photosynthesis and partitioning of available energy. part I: Model description and comparison with a multi-layered model, *Agric. Forest Meteorol.*, *91*, 89–111.
- Williams, R. J., G. A. Duff, M. J. S. D. Bowman, and G. D. Cook (1996), Variation in the composition and structure of tropical savannas as a function of rainfall and soil texture along a large-scale climatic gradient in the Northern Territory, Australia, *J. Biogeogr.*, *23*, 747–756.
- Wullschlegel, S. D., T. J. Tschaplinski, and R. J. Norby (2002), Plant water relations at elevated CO<sub>2</sub> - Implications for water-limited environments, *Plant Cell Environ.*, *25*, 319–331.
- Wythers, K. R., W. K. Lauenroth, and J. M. Paruelo (1999), Bare-soil evaporation under semiarid field conditions, *Soil Sci. Soc. Am. J.*, *63*, 1341–1349.
- Zavaleta, E. S., M. R. Shaw, N. R. Chiariello, B. D. Thomas, E. E. Cleland, C. B. Field, and H. A. Mooney (2003), Grassland responses to three years of elevated temperature, CO<sub>2</sub>, precipitation, and N deposition, *Ecol. Monogr.*, *73*, 585–604.
- Zhou, X., X. Liu, L. L. Wallace, and Y. Luo (2007), Photosynthetic and respiratory acclimation to experimental warming for four species in a tallgrass prairie ecosystem, *J. Integr. Plant Biol.*, *49*, 270–281.

Y. Luo and E. Weng, Department of Botany and Microbiology, University of Oklahoma, 770 Van Vleet Oval, Norman, OK 73019-6131, USA. (yluo@ou.edu; esweng@ou.edu)